1996ApJ...468..543F

THE ASTROPHYSICAL JOURNAL, 468:543–555, 1996 September 10
No copyright is claimed for this article. Printed in U.S.A.

VLBI OBSERVATIONS OF EIGHT EXTREME SCATTERING EVENT SOURCES: MILLIARCSECOND-SCALE STRUCTURE

ALAN L. FEY
United States Naval Observatory, Code EO, 3450 Massachusetts Avenue NW, Washington, DC 20392-5420; afey@alf.usno.navy.mil
ANDREW W. CLEGG
Naval Research Laboratory, Code 7213, Washington, DC 20375-5351; clegg@rira.nrl.navy.mil
AND
RALPH L. FIEDLER
Naval Research Laboratory, Code 7261, Washington, DC 20375-5351; fiedler@sealab.nrl.navy.mil
Received 1996 January 5; accepted 1996 April 2

ABSTRACT

We present multiple-epoch, multiple-frequency VLBI observations of eight extragalactic sources whose radio light curves have undergone an extreme scattering event (ESE). The VLBI observations were made at times during which the sources were not undergoing ESE events. The eight sources show relatively simple intrinsic structure, with one or two dominant components containing the majority of the total flux density, and component angular sizes on the order of several milliarcseconds. We have interpreted the ESE light curves for these sources in the context of a simple statistical scattering model. There appears to be no direct correspondence between intrinsic source structure and the form of the radio light curves during an ESE. Our results suggest that some of the variations in the radio light curves of these sources are due to the complexity of the scattering medium itself.

Subject headings: radio continuum: galaxies — scattering

1. INTRODUCTION

Extreme Scattering Events (ESEs) are a form of extreme variation in the radio light curves of a number of extragalactic sources (Fiedler et al. 1987). These peculiar variations have a strong frequency dependence (ESEs identified at 2 GHz usually have no counterpart at 8 GHz) and no resemblance either to intrinsic flux density variations normally observed in a given source or to normal refractive interstellar scintillation (RISS).

ESEs have generally been attributed to propagation effects produced by electron density fluctuations in the intervening interstellar medium (ISM). Several models have been developed to describe ESEs, such as the Gaussian lens model of Romani, Blandford, & Cordes (1987), which relies on a localized structure in the ISM with a smooth, Gaussian profile of excess electron density, or the Fiedler et al. (1994a, hereafter FDJWS) model, in which ray path distortions are produced by a large number of electron density fluctuations confined to a localized region of the ISM. To date, the true nature of the electron density enhancements remains to be resolved.

A total of 11 ESEs have been tentatively identified in the 2 GHz light curves of 10 extragalactic sources (cf. FDJWS; Clegg, Fey, & Fiedler 1996). FDJWS suggest that ESEs appear to occur in the light curves of sources whose lines of sight are preferentially located near loops in the Galactic foreground brightness distribution. Fiedler et al. (1994b) find that the lines of sight toward three of the ESE sources pass through the edges of clearly identifiable Galactic structures. These structures are possible sites for enhanced electron density turbulence.

In this paper, we present multiple-epoch, multiple-frequency Very Long Baseline Interferometry (VLBI) observations of eight extragalactic sources whose light curves have exhibited ESEs. The VLBI observations were made at times during which the sources were not undergoing ESE events. Consequently, source structure information derived from these data should be mostly intrinsic. The simple ESE model presented by FDJWS is based on strong scattering by a Galactic region of high electron density turbulence, which has an angular extent comparable to that of the background source. Using the intrinsic structure information obtained from the VLBI data, we make a qualitative comparison between the milliarcsecond-scale structure of these sources and their ESE radio light curves in the context of the FDJWS scattering model.

2. OBSERVATIONS AND DATA ANALYSIS

Observations were made at three epochs using VLBI. The first epoch observations were carried out on 1988 May 27 using the standard Mark II VLBI recording system at a frequency of 1.66 GHz. The participating observatories are listed in Table 1. Only two of the eight ESE sources (0300+470 and 1749+096) were observed during this session, with limited (u, v) coverage. Second epoch observations were made on 1989 April 11, again using the standard Mark II VLBI recording system, but at a frequency of 4.99 GHz. Antennas used for this session are also listed in Table 1. In the second session all eight sources were observed using 30 minute scans over a number of different hour angles in order to maximize the (u, v) coverage. The (assumed) unresolved source 0235+164 was also observed in both sessions in order to aid in the initial amplitude calibration of the Mark II visibility data. The third epoch observations were made on 1994 July 8 using the Very Long Baseline Array (VLBA) telescope (Napier et al. 1994) of the National Radio Astronomy Observatory (NRAO).[1] Eight

[1] NRAO is operated by Associated Universities, Inc., under cooperative agreement with the National Science Foundation.

© American Astronomical Society • Provided by the NASA Astrophysics Data System

1996ApJ...468..543F

TABLE 1

MARK II VLBI STATIONS

Location	Session
Bologna, Italy	1989 April
Effelsberg, West Germany	1988 May/1989 April
Fort Davis, TX	1988 May/1989 April
Westford, MA	1988 May/1989 April
North Liberty, IA	1988 May/1989 April
Jodrell Bank, England	1989 April
Green Bank, WV	1988 May/1989 April
Maryland Point, MD	1988 May/1989 April
Owens Valley, CA	1988 May/1989 April
Pietown, NM	1988 May
Socorro, NM	1989 April
Westerbork, The Netherlands	1989 April

frequency channels were recorded, each 4 MHz wide, with 4 at S band (centered at 2.22, 2.23, 2.29, and 2.32 GHz) and 4 at X band (centered at 8.15, 8.23, 8.41, and 8.55 GHz) for a total bandwidth of 16 MHz in each band. Six of the eight ESE sources (0300+470, 1502+106, 1611+343, 1741−038, 1749+096, and 1821+107) were observed during this session. Sources were observed using 4 minute scans over a number of different hour angles. This last observing program included a total of 42 sources. The six sources discussed here were observed for about 4 to 5 scans each. The remaining sources observed during this session were for a different project and are not relevant to this paper. Results of the remaining observations will be presented elsewhere (cf. Fey, Clegg, & Fomalont 1996).

The Mark II videotapes were correlated with the CIT/JPL Block II correlator at the California Institute of Technology. The VLBA data were correlated with the VLBA correlator at the Array Operations Center in Socorro, New Mexico. The correlated data were processed with the NRAO Astronomical Image Processing System (AIPS) global fringe-fitting software. Fringe-fitting intervals of 6 minutes were used for the Mark II data, while intervals of 1 minute were used for the VLBA data. After correction for residual delay and rate, the 2 s correlator records were coherently averaged. The Mark II data were averaged to 60 s records, and the VLBA data were averaged to 10 s records. The data were then edited. The calibrated visibility data were Fourier inverted using natural weighting and then CLEANed in the standard manner. The Caltech VLBI mapping software, including DIFMAP, was used throughout. For the VLBA data, the four frequency channels in each band were combined in the (u, v) plane during gridding, taking into account the frequency differences. For convenience, the resulting VLBA images for each band will be referred to only by a single fiducial frequency (2.32 GHz and 8.55 GHz, respectively) even though they were made using the data from all frequency channels. The data were also self-calibrated using the hybrid-mapping technique (Pearson & Readhead 1984) to correct for residual amplitude and phase errors. A point source was used as a starting model for the iterative self-calibration and mapping procedure in all cases. Convergence was usually obtained in less than 10 iterations. Contour plots of the final images are shown in Figures 1 through 8. Tables 2, 3, and 4 list the parameters of the final images.

To obtain source parameters for subsequent analysis, we performed least-squares fits of Gaussian components to the *self-calibrated* visibility data. Results of the model fitting are listed in Table 5. In this table, the first column lists the source name. The second and third columns list the epoch and frequency of observation. The fourth through tenth columns list the results of the model fitting, which are, respectively, the reference number of each Gaussian component fitted to the data, the integrated flux density of the fitted components, the angular separation of the model components from an arbitrary origin (the first component listed is always assumed to be at the origin), the position angle of a line joining the components with the origin of the image (measured north through east), the angular size (FWHM major axis) of the model components, the axial ratio (the minor axis divided by the major axis) of the components, and the position angle of the major axis of the components (measured north through east). The eleventh column lists the reduced χ^2 between the model and the visibility data. The reduced χ^2 has an expected value of 1.0 (however, when the data are self-calibrated, the number of degrees of freedom is reduced, so that the expected value of the reduced χ^2 may actually be significantly less than 1.0; cf. Henstock et al. 1995).

Although the agreement between the fitted models and the data is not as good as that produced by the hybrid images (models with many CLEAN components), inspection of plots of residuals in the image plane, after subtracting the Gaussian models from the visibility data, revealed that the Gaussian models generally describe the visibility data quite well, with typical peak residuals of approximately 10 σ. However, because of incomplete sampling in the (u, v) plane, these models may not be unique. They represent only one *possible* deconvolution of complex source structure. Such deconvolutions can be misleading.

TABLE 2

IMAGE PARAMETERS FOR SESSION 1988 MAY

Source	ν (GHz)	Beam[a] a (mas)	Beam[a] b (mas)	Beam[a] ϕ	Peak (Jy beam^{-1})	rms[b] (mJy beam^{-1})	Contour Levels[c] (mJy beam^{-1})
0300+470	1.66	7.2	5.4	−42°	1.94	1.4	$5.6 \times (1, \ldots, 2^8)$
1749+096	1.66	26.4	7.2	−11	0.96	0.8	$2.3 \times (1, \ldots, 2^8)$

[a] The restoring beam is an elliptical Gaussian with FWHM major axis a and minor axis b, with major axis in position angle ϕ (north through east).

[b] The root mean square of the residuals of the final hybrid image.

[c] Contour levels are represented by the geometric series $1, \ldots, 2^n$; e.g., for $n = 5$ the contour levels would be $\pm 1, 2, 4, 8, 16, 32$.

© American Astronomical Society • Provided by the NASA Astrophysics Data System

1996ApJ...468..543F

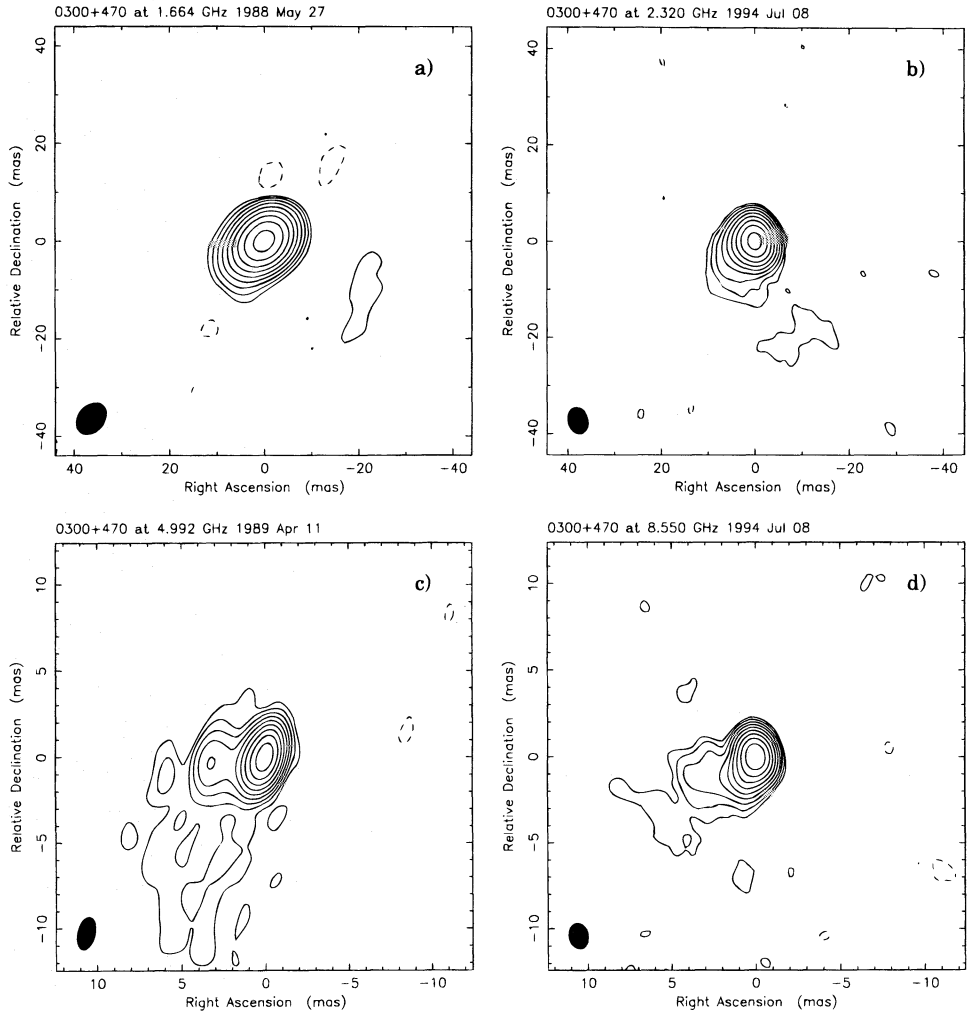

FIG. 1.—Contour plots of the radio source 0300+470 at 1.66 GHz, 2.32 GHz, 4.99 GHz, and 8.55 GHz. Map parameters are listed in Tables 2, 3, and 4. Gaussian models fitted to the visibility data are listed in Table 5. The FWHM restoring beam applied to the images is shown as an ellipse in the lower left-hand side of each panel.

We have, therefore, not attempted to estimate errors for the model parameters. We now discuss the intrinsic structure of each source separately.

2.1. *0300+470*

The BL Lac object 0300+470 (4C +47.08) has a redshift of 0.475 (Hughes, Aller, & Aller 1992). This source was previously known to be highly compact (Weiler & Johnston 1980; Lawrence et al. 1985), but VLBI images have only recently become available. Gabuzda et al. (1992) found the dominant 4.99 GHz structure at epoch 1987 May to be a close double in position angle ~86° with a resolved component of about 3 mas from the core.

Our images of 0300+470 are shown in Figure 1. These

TABLE 3

IMAGE PARAMETERS FOR SESSION 1989 APRIL

Source	ν (GHz)	Beam[a] a (mas)	b (mas)	ϕ	Peak (Jy beam^{-1})	rms[b] (mJy beam^{-1})	Contour Levels[c] (mJy beam^{-1})
0300+470.....	4.99	1.9	1.0	−14°	1.34	1.1	$3.2 \times (1, \ldots, 2^8)$
0333+321.....	4.99	3.3	1.1	−22	0.78	1.5	$5.1 \times (1, \ldots, 2^7)$
1502+106.....	4.99	10.0	0.8	−10	1.45	2.0	$4.1 \times (1, \ldots, 2^8)$
1611+343.....	4.99	4.4	0.8	−5	1.98	2.8	$7.0 \times (1, \ldots, 2^7)$
1741−038.....	4.99	12.3	0.9	−8	2.38	1.5	$4.6 \times (1, \ldots, 2^9)$
1749+096.....	4.99	9.1	0.9	−11	1.39	1.5	$3.9 \times (1, \ldots, 2^8)$
1821+107.....	4.99	8.3	1.0	−11	0.93	1.1	$3.4 \times (1, \ldots, 2^8)$
2352+495.....	4.99	3.4	1.0	−9	0.45	1.6	$7.8 \times (1, \ldots, 2^5)$

[a] The restoring beam is an elliptical Gaussian with FWHM major axis a and minor axis b, with major axis in position angle ϕ (north through east).

[b] The root mean square of the residuals of the final hybrid image.

[c] Contour levels are represented by the geometric series $1, \ldots, 2^n$; e.g., for $n = 5$ the contour levels would be $\pm$ 1, 2, 4, 8, 16, 32.

© American Astronomical Society • Provided by the NASA Astrophysics Data System

1996ApJ...468..543F

TABLE 4

IMAGE PARAMETERS FOR SESSION 1994 JULY

Source	ν (GHz)	Beam[a] a (mas)	Beam[a] b (mas)	Beam[a] ϕ	Peak (Jy beam^{-1})	rms[b] (mJy beam^{-1})	Contour Levels[c] (mJy beam^{-1})
0300+470.....	2.32	5.6	4.2	17°	0.96	0.9	$2.8 \times (1, \ldots, 2^8)$
	8.55	1.5	1.2	15	0.91	0.6	$1.8 \times (1, \ldots, 2^8)$
1502+106.....	2.32	7.2	3.8	−1	1.81	1.2	$3.7 \times (1, \ldots, 2^8)$
	8.55	1.9	1.0	−1	1.38	1.2	$3.6 \times (1, \ldots, 2^8)$
1611+343.....	2.32	5.6	3.7	−1	3.38	2.3	$9.1 \times (1, \ldots, 2^8)$
	8.55	1.5	1.0	−2	2.10	1.2	$3.6 \times (1, \ldots, 2^9)$
1741−038.....	2.32	7.9	3.6	0	2.07	1.2	$3.7 \times (1, \ldots, 2^9)$
	8.55	2.1	1.0	0	2.84	1.2	$4.1 \times (1, \ldots, 2^9)$
1749+096.....	2.32	7.2	3.4	−4	1.36	1.2	$3.7 \times (1, \ldots, 2^8)$
	8.55	2.0	0.9	−4	2.71	1.2	$3.5 \times (1, \ldots, 2^9)$
1821+107.....	2.32	7.3	4.0	−5	1.25	1.0	$3.0 \times (1, \ldots, 2^8)$
	8.55	2.0	1.1	−4	0.49	0.8	$2.3 \times (1, \ldots, 2^7)$

[a] The restoring beam is an elliptical Gaussian with FWHM major axis a and minor axis b, with major axis in position angle ϕ (north through east).

[b] The root mean square of the residuals of the final hybrid image.

[c] Contour levels are represented by the geometric series $1, \ldots, 2^n$; e.g., for $n = 5$ the contour levels would be $\pm$ 1, 2, 4, 8, 16, 32.

images show a compact asymmetric source. The data at each frequency show multiple components with a dominant core containing about 80% of the total flux density and weaker, more extended emission to the southeast of the core. The structure at 4.99 GHz is consistent with that found by Gabuzda et al. (1992) approximately two years earlier. The 4.99 GHz model listed in Table 5 accounts for 100% of the single dish flux density measured at Effelsberg and Owens Valley during the Mark II observations, suggesting that there is little extended emission at this frequency.

2.2. *0333+321*

The quasar 0333+321 (NRAO 140) has a redshift of 1.263 (Hewitt & Burbidge 1993). Previous images of this source (Marscher 1988) show a multiple-component core-jet structure, with the two components closest to the core separating superluminally from the core. The source shows low-frequency variability (Marscher et al. 1987), and there is no evidence for arcsecond-scale structure (Browne et al. 1982).

Our 4.99 GHz image of 0333+321 is shown in Figure 2. This image shows a complex source. The data show a core-jet structure with multiple jet components, a result consistent with that of Marscher (1988). We find that about 80% of the total flux density is contained within three central components (within a region $\lesssim$3 mas). These three components are quite compact, each with an angular size less than 1 mas. The total 4.99 GHz model flux density accounts for 100% of the single-dish flux density measured at Effelsberg, Owens Valley, and Westerbork during the Mark II observations.

2.3. *1502+106*

The quasar 1502+106 (4C 10.39) has a redshift of 1.839 (Hewitt & Burbidge 1993). The VLBI data of Spangler et al. (1981) indicates a core-halo structure for this source with a compact (angular size less than 1 mas) component dominating the source at both 4.99 GHz and 1.66 GHz. Zensus, Porcas, & Pauliny-Toth (1984) found that about 78% of the total flux density was contained in a compact component of approximately 0.8 mas diameter at 4.99 GHz.

Our images of 1502+106 are shown in Figure 3. These images show a compact asymmetric source. The data at each frequency show multiple components with a dominant core containing more than 75% of the total flux density and weaker, more extended emission approximately due east of the core. The compact structure at 4.99 GHz is consistent with that found by Zensus et al. (1984). The fitted 4.99 GHz model accounts for 100% of the single-dish flux density measured at Owens Valley and Westerbork during the Mark II observations.

2.4. *1611+343*

The quasar 1611+343 (DA 406) has a redshift of 1.401 (Hewitt & Burbidge 1993). Romney et al. (1984) report that about 80% of the total flux density at 1.67 GHz is contained within an unresolved (angular size $\leq$3 mas) component. The source shows low-frequency variability (Altschuler et al. 1984) with characteristics indicative of RISS (Dennison et al. 1984).

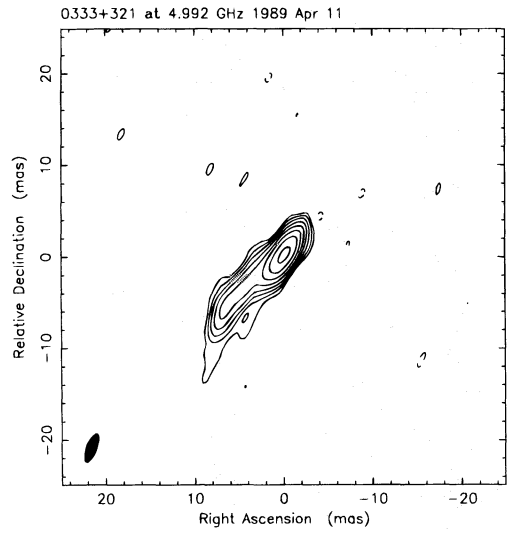

FIG. 2.—Contour plot of the radio source 0333+321 at 4.99 GHz. Map parameters are listed in Table 3. A Gaussian model fitted to the visibility data is listed in Table 5. The FWHM restoring beam applied to the image is shown as an ellipse in the lower left-hand side of the panel.

© American Astronomical Society • Provided by the NASA Astrophysics Data System

1996ApJ...468..543F

TABLE 5

GAUSSIAN MODELS[a]

Source	Session	ν (GHz)	Component	S (Jy)	r (mas)	θ	a (mas)	b/a	ϕ	χ^2
0300+470.....	1988 May	1.66	1	1.78	0.0	...	1.75	0.69	90°	0.81
			2	0.39	2.4	104°	2.49	1.00	...	
			3	0.06	7.5	134	5.38	1.00	...	
	1994 July	2.32	1	0.95	0.0	...	1.57	0.09	−37	0.88
			2	0.14	2.6	109	2.13	1.00	...	
			3	0.05	6.4	128	5.88	1.00	...	
	1989 April	4.99	1	1.33	0.0	...	0.50	0.52	−46	0.71
			2	0.28	0.9	124	0.90	1.00	...	
			3	0.11	3.1	94	1.43	1.00	...	
	1994 July	8.55	1	0.89	0.0	...	0.21	0.45	−36	0.84
			2	0.12	1.0	152	0.26	1.00	...	
			3	0.05	1.5	148	0.74	1.00	...	
			4	0.05	3.0	114	2.62	1.00	...	
0333+321.....	1989 April	4.99	1	0.64	0.0	...	0.54	1.00	...	1.28
			2	0.48	1.4	−52	0.55	1.00	...	
			3	0.34	1.5	126	0.90	1.00	...	
			4	0.17	4.9	127	0.99	1.00	...	
			5	0.20	8.3	131	1.48	1.00	...	
1502+106.....	1994 July	2.32	1	1.64	0.0	...	0.95	0.13	−44	0.83
			2	0.30	1.7	119	1.55	1.00	...	
			3	0.17	6.6	81	5.29	1.00	...	
			4	0.02	8.9	140	1.31	1.00	...	
	1989 April	4.99	1	1.90	0.0	...	0.73	1.00	...	1.27
			2	0.09	3.0	70	0.50	1.00	...	
	1994 July	8.55	1	1.38	0.0	...	0.45	0.22	−39	0.86
			2	0.24	0.9	126	0.55	1.00	...	
			3	0.11	2.0	134	0.97	1.00	...	
			4	0.11	3.0	97	5.72	1.00	...	
1611+343.....	1994 July	2.32	1	4.16	0.0	...	2.98	0.50	−20	1.46
	1989 April	4.99	1	1.93	0.0	...	1.51	0.24	−4	1.58
			2	1.09	2.0	164	1.55	1.00	...	
	1994 July	8.55	1	2.14	0.0	...	0.38	0.00	−9	1.04
			2	0.35	1.5	−178	0.47	1.00	...	
			3	0.65	2.6	172	0.98	1.00	...	
			4	0.37	3.3	156	1.34	1.00	...	
1741−038.....	1994 July	2.32	1	2.09	0.0	...	0.51	1.00	...	0.94
			2	0.04	9.0	172	6.30	1.00	...	
	1989 April	4.99	1	2.45	0.0	...	0.42	1.00	...	0.98
			2	0.28	1.0	171	1.72	1.00	...	
	1994 July	8.55	1	2.24	0.0	...	0.00	1.00	...	0.93
			2	0.75	0.3	−169	0.55	1.00	...	
1749+096.....	1988 May	1.66	1	0.99	0.0	...	2.13	1.00	...	0.49
			2	0.05	9.8	38	5.44	1.00	...	
	1994 July	2.32	1	1.37	0.0	...	1.06	0.00	54	0.76
			2	0.10	3.1	30	0.53	1.00	...	
			3	0.05	7.8	34	4.37	1.00	...	
	1989 April	4.99	1	1.51	0.0	...	0.67	0.42	18	0.65
			2	0.09	1.5	28	0.67	1.00	...	
			3	0.06	4.0	33	1.54	1.00	...	
	1994 July	8.55	1	2.73	0.0	...	0.18	0.47	28	0.86
			2	0.11	2.0	26	1.56	1.00	...	
1821+107.....	1994 July	2.32	1	1.29	0.0	...	1.60	0.14	−24	0.87
			2	0.05	12.4	−1	3.42	1.00	...	
			3	0.04	28.7	−9	8.55	1.00	...	
	1989 April	4.99	1	0.92	0.0	...	1.06	0.35	−22	0.55
			2	0.15	1.8	−19	0.99	1.00	...	
	1994 July	8.55	1	0.50	0.0	...	0.79	0.00	−19	0.80
			2	0.18	1.6	−15	0.40	1.00	...	
			3	0.03	2.5	−20	0.51	1.00	...	
2352+495.....	1989 April	4.99	1	0.60	0.0	...	1.60	1.00	...	2.15
			2	0.31	2.3	173	0.49	1.00	...	
			3	0.14	16.3	−21	1.36	1.00	...	
			4	0.14	32.2	165	5.73	1.00	...	

[a] The models fitted to the visibility data are of Gaussian form with flux density S, FWHM major axis a, and minor axis b, with major axis in position angle ϕ (measured north through east). Components are separated from an arbitrary origin by a distance r along position angle θ, which is the position angle (measured north through east) of a line joining the components with the origin.

© American Astronomical Society • Provided by the NASA Astrophysics Data System

1996ApJ...468..543F

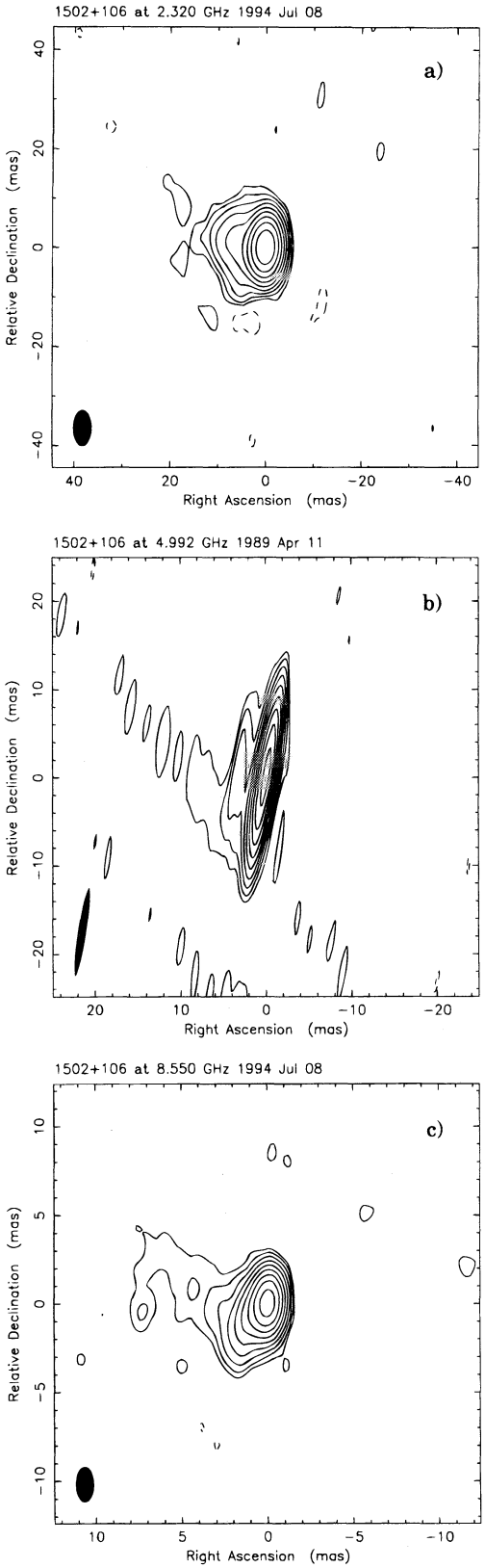

FIG. 3.—Contour plots of the radio source 1502+106 at 2.32 GHz, 4.99 GHz, and 8.55 GHz. Map parameters are listed in Tables 3 and 4. Gaussian models fitted to the visibility data are listed in Table 5. The FWHM restoring beam applied to the images is shown as an ellipse in the lower left-hand side of each panel.

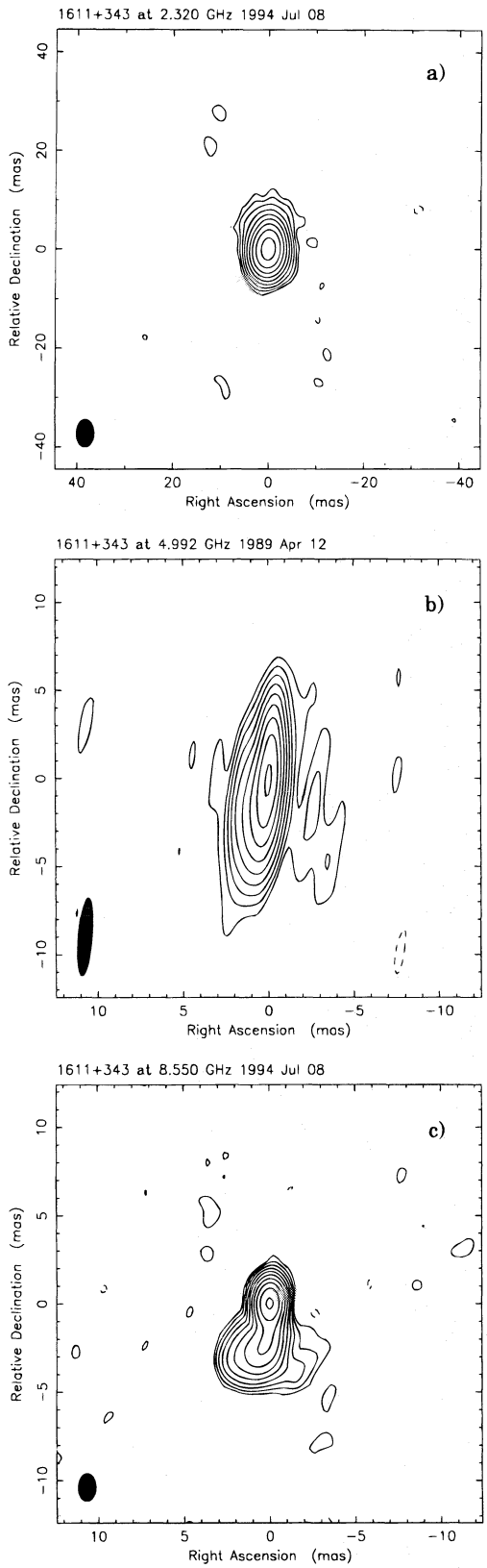

FIG. 4.—Same as Fig. 3, except for the source 1611+343

Our images of 1611+343 are shown in Figure 4. These images show a simple source structure at 2.32 GHz that becomes more complex at the higher frequencies. The 2.32 GHz data show an elongated naked core object with angular size $\lesssim 3$ mas, a result consistent with that of Romney et al. (1984). At 4.99 GHz and 8.55 GHz the data show multiple components, with a dominant core containing about 60% of the total flux density and weaker, more extended emission approximately due south of the core. The

© American Astronomical Society • Provided by the NASA Astrophysics Data System

1996ApJ...468..543F

4.99 GHz model accounts for 100% of the single-dish flux density measured at Effelsberg and Owens Valley during the Mark II observations.

2.5. *1741−038*

The quasar 1741−038 has a redshift of 1.057 (Véron-Cetty & Véron 1993). Our images of 1741−038 are shown in Figure 5. These images show a simple compact source. The data at each frequency show two components dominated by a central compact core containing the majority of the total flux density. The data at each frequency also show weaker, more extended emission to the south of the core, which becomes more prominent at the higher frequencies. The 4.99 GHz model accounts for 100% of the single-dish flux density measured at Effelsberg, Owens Valley, and Westerbork during the Mark II observations.

2.6. *1749+096*

The redshift of the BL Lac object 1749+096 (4C +09.57) is 0.32 (Stickel, Fried, & Kuehr 1993). Weiler & Johnston (1980) found that at least 90% of the 4.99 GHz flux density of 1749+096 is contained within a compact component of angular size ~0.2 mas. Wehrle et al. (1992) find that at 4.99 GHz the source has a strong central peak with extensions to the north. The source is known to have very little arcsecond-scale structure (Antonucci & Ulvestad 1985).

Our images of 1749+096 are shown in Figure 6. These images show an asymmetric compact source. The data at each frequency show multiple components dominated by a central compact core containing more than 90% of the total flux density, a result consistent with that of Weiler & Johnston (1980). The data at each frequency also show weaker, more extended emission to the northeast of the core, a result consistent with that of Wehrle et al. (1992). The 4.99 GHz model listed in Table 5 accounts for 100% of the single-dish flux density measured at Effelsberg, Owens Valley, and Westerbork during the Mark II observations.

2.7. *1821+107*

The redshift of the quasar 1821+107 is 1.364 (Hewitt & Burbidge 1993). Our images of 1821+107 are shown in Figure 7. These images show an asymmetric compact source. The data at each frequency show multiple components dominated by a central compact core containing the majority of the total flux density. The data at each frequency also show weaker, more extended emission to the north of the core, which becomes more prominent at the higher frequencies. The 4.99 GHz model accounts for 100% of the single-dish flux density measured at Effelsberg, Owens Valley, and Westerbork during the Mark II observations.

2.8. *2352+495*

The radio galaxy 2352+495 (DA 611) has a redshift of 0.237 (O'Dea, Baum, & Stanghellini 1991). Pearson & Readhead (1988) and Conway et al. (1992) have previously imaged this source at 4.99 GHz. Their images show a complex structure surrounding a compact core. Wilkinson et al. (1994) have imaged this source at 1.67 GHz. They classify the source as a two-sided compact symmetric object. No radio structure on scales larger than 0.″2 has been detected for this source (Perley 1982).

Shown in Figure 8 is our 4.99 GHz image of 2352+495. This image shows a complex source. The data show multiple components dominated by a compact core, a result consistent with that of Pearson & Readhead (1988) and Conway et al. (1992). We find that about 75% of the total flux density is contained in two components within the central core (within a region of about 2 mas). The fitted

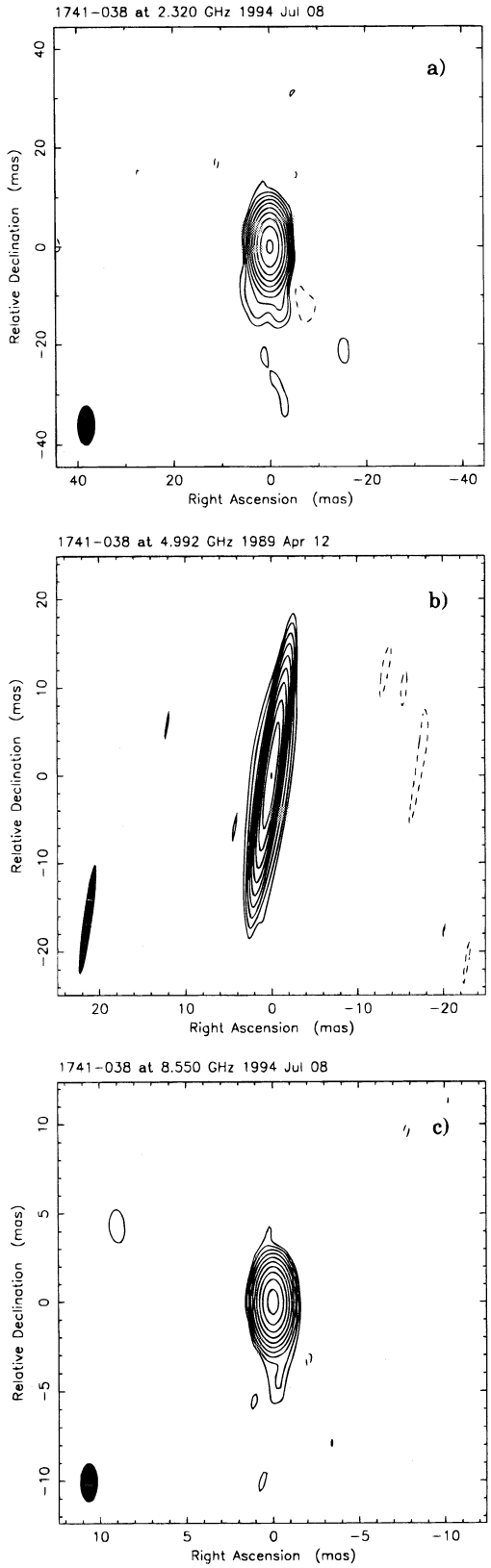

FIG. 5.—Same as Fig. 3, except for the source 1741−038

© American Astronomical Society • Provided by the NASA Astrophysics Data System

1996ApJ...468..543F

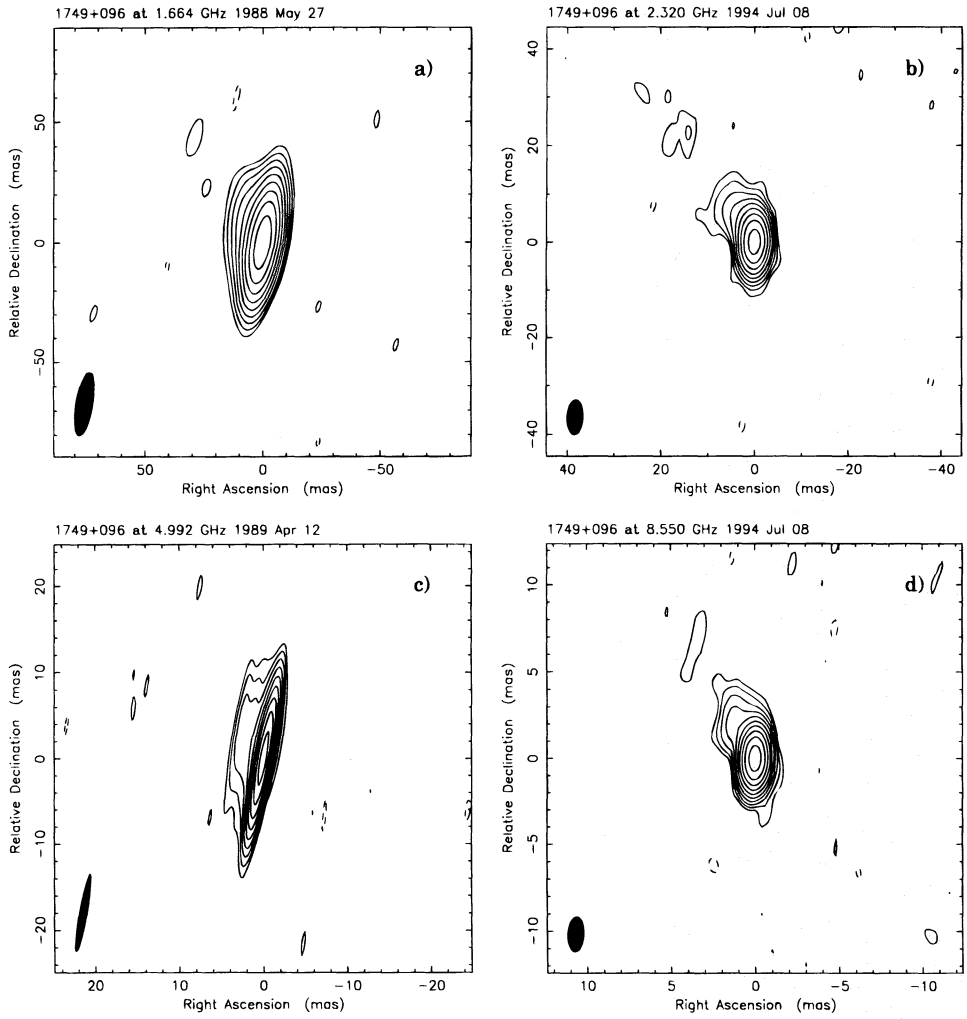

FIG. 6.—Same as Fig. 1, except for the source 1749+096

model listed in Table 5 has a reduced $\chi^2 \approx 2.15$, suggesting that the model is probably not a very good representation of the source structure. In addition, the total model flux density accounts for only about 85% of the single-dish flux density measured at Effelsberg, Owens Valley, and Westerbork during the Mark II observations, suggesting that significant extended emission has been completely resolved by the current observations.

3. COMPARISON OF INTRINSIC STRUCTURE WITH EXTREME SCATTERING EVENT LIGHT CURVES

In this section we make a comparison of the complexity of the VLBI structure of the eight observed sources with the complexity of the temporal variations in the light curves for these same sources during an ESE event. The VLBI observations were made at times during which the sources were not undergoing ESE events. Consequently, source structure information derived from these data should be mostly intrinsic. We have estimated the contribution that normal diffractive interstellar broadening will have on source sizes using the Taylor & Cordes (1993) model and conclude that diffractive broadening is not a significant factor for these ESE sources. Along the lines of sight to these sources, less than 0.5 mas of diffractive broadening is expected.

In defining complexity in the radio light curves, we are referring to how much the light curves differ from the light curves predicted by simple models for ESEs, such as those of Romani et al. (1987), Romani (1988), Clegg, Chernoff, & Cordes (1988), and FDJWS. The comparison will be mostly qualitative and will be limited to comparison of the 2.32 GHz source structure with the 2.25 GHz light curves, since ESE effects are much more pronounced at lower frequencies. Also, many of the sources either do not have 4.99 GHz light curves available or do not exhibit ESE-like fluctuations in their light curves at this higher frequency.

For the sources 0333+321 and 2352+495, we only acquired VLBI data at 4.99 GHz. For interpretation of these sources we have scaled their 4.99 GHz structure to 2.25 GHz. We have assumed that the component separations at 2.25 GHz are the same as at 4.99 GHz, but the angular sizes of the components are larger by a factor of 2.2. This follows from assuming that the source size of flat-spectrum extragalactic radio sources scales as λ.

The light curves for each of the sources during their respective scattering events are shown in Figure 9. We reproduce here light curves only at 2.25 GHz. The reader is referred to FDJWS for a thorough discussion of these ESE light curves and a complete set, including those at 8.1 GHz. The bold horizontal line in each panel in Figure 9 identifies the period of time during which the source appears to be

© American Astronomical Society • Provided by the NASA Astrophysics Data System

1996ApJ...468..543F

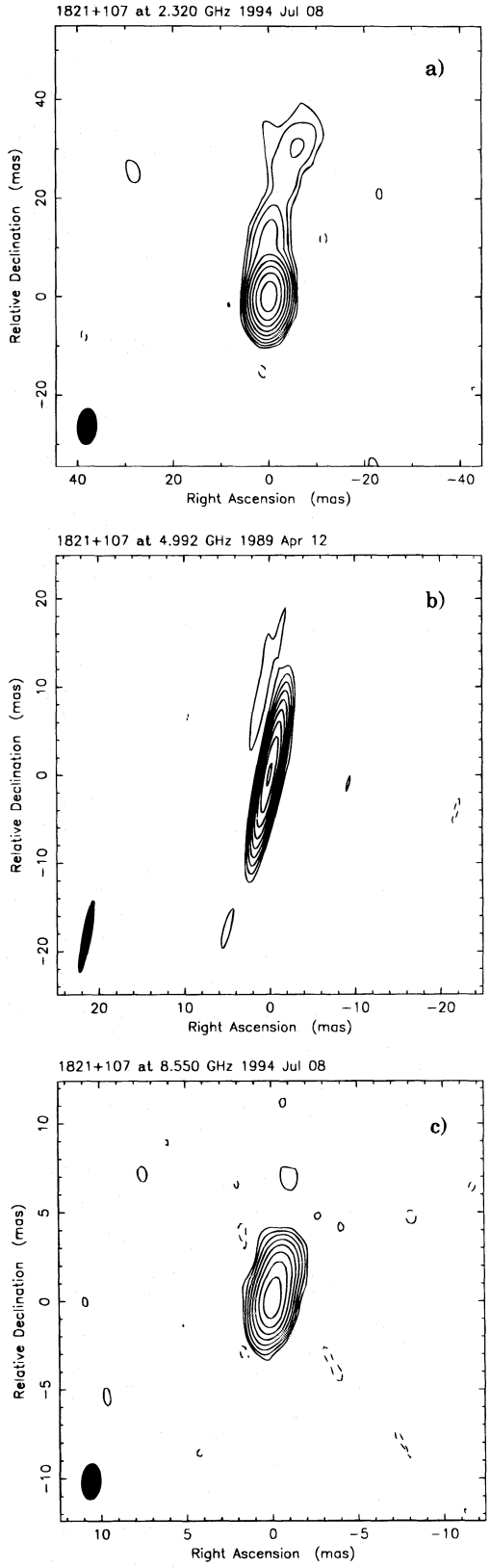

FIG. 7.—Same as Fig. 3, except for the source 1821+107

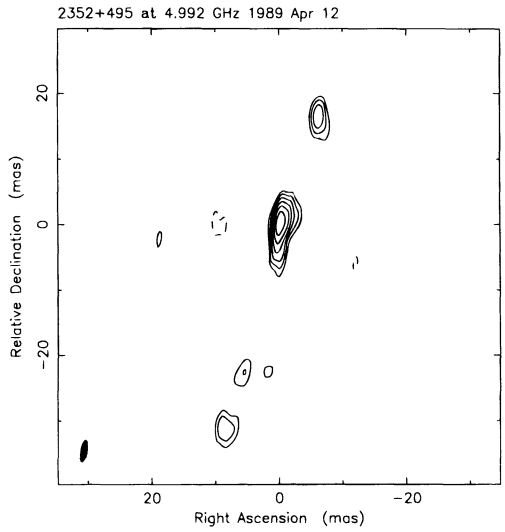

FIG. 8.—Same as Fig. 2, except for the source 2352+495

undergoing an ESE. In the following discussion, we will compare these light curves to those predicted by the statistical scattering model derived by FDJWS. In this model, the scattering is produced by a discrete structure in which there are many large-amplitude fluctuations of electron density. The inhomogeneities throughout the structure are assumed to redistribute the radiation from a point source into a Gaussian distribution of angles. It is also assumed that the broadening angle is constant across the extent of the scattering lens.

We emphasize that only qualitative comparisons are made. We have attempted not to overanalyze our data because of the large number of unknown parameters and because the true nature of ESEs is so poorly understood.

3.1. *0300+470*

The light curve for this source cannot be fitted well by any simple model for ESEs. The VLBI data show a dominant source component that contains about 83% of the total flux density at 2.32 GHz. Simulations show that a complex light curve is not expected in the case in which a single source component contains the majority of the total flux density. This is illustrated in Figures 10 and 11, which show light curves generated using the model of FDJWS. Two general cases are considered: Figure 10, in which the angular size of the scattering lens is similar to the angular size of the background source (i.e., the rounded minimum case of FDJWS), and Figure 11, in which the angular size of the lens is larger than the angular size of the background source (i.e., the flat minimum case of FDJWS). The different curves within each panel represent the expected light curves for a single lens imaging a source with two closely spaced components. The different panels within each plot represent different angular separations for the two source components. The lens is assumed to move sequentially across the two source components. As can be seen, the model fails to qualitatively reproduce the observed light curve of 0300+470, which exhibits numerous large-amplitude variations during the ESE.

It is possible that the structure of the lens itself is complex, which gives rise to the complexity of the light curve. To lowest order, the light curve produced by two closely spaced lenses is similar to that of a single lens imaging a source with two closely spaced components. The different panels within Figures 10 and 11 show light curves in which the separation between two source components

© American Astronomical Society • Provided by the NASA Astrophysics Data System

1996ApJ...468..543F

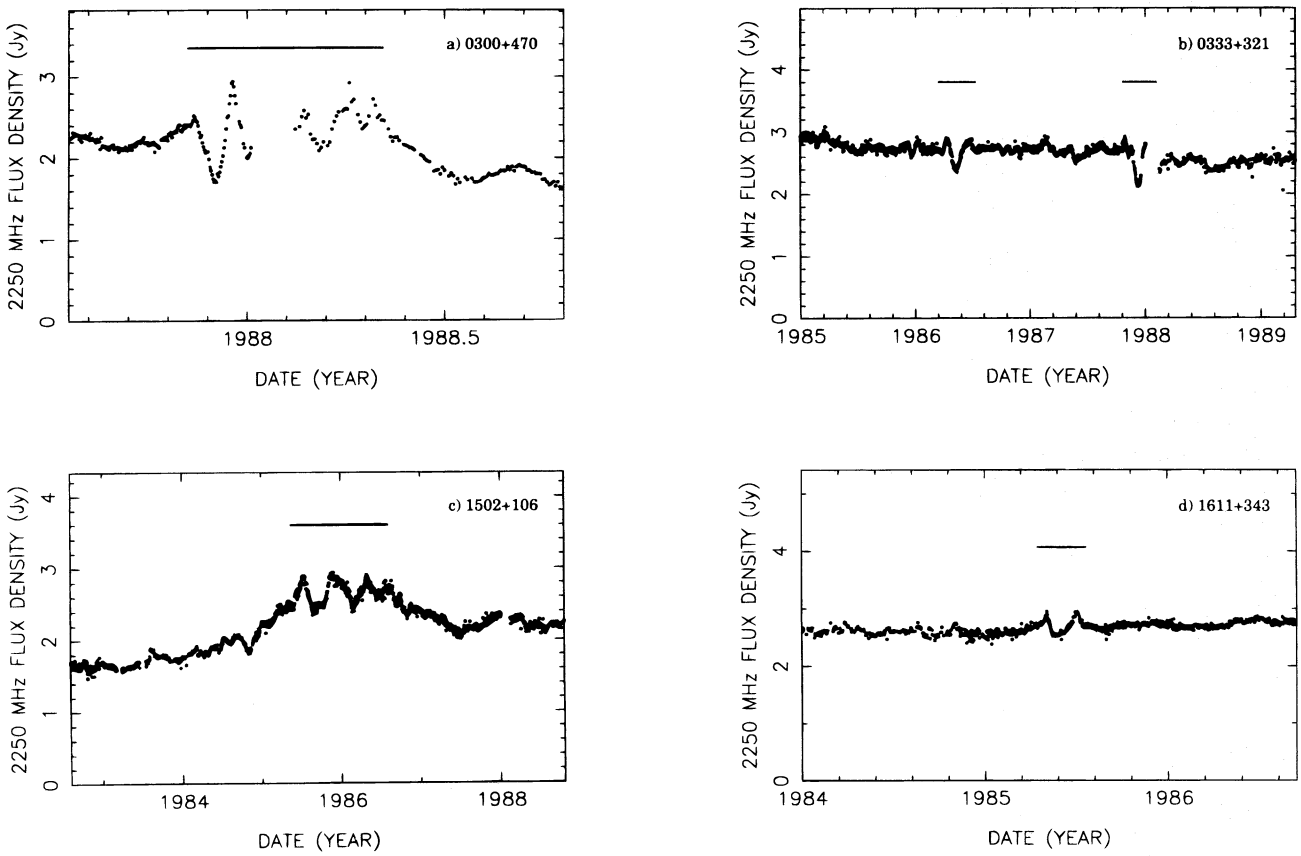

FIG. 9.—Radio frequency light curves for eight sources that show extreme scattering events (ESEs). The variations associated with an ESE are clearly atypical of the variations normally observed in these sources. The time frame for each ESE is indicated by a bold horizontal line in each panel. The reader is referred to Fiedler et al. (1994a) for a more complete discussion of these light curves.

(or, equivalently, the separation between two closely spaced lenses) increases from being less than the angular size of the scattering lens to being greater than the angular size of the scattering lens. The case in which the two source components are of equal flux density (*dotted curves*) can qualitatively approximate the multiple variations seen in the 2.25 GHz light curve of 0300+470. This would be similar to the case in which two closely spaced lenses pass over a background source with a single dominant component. Given the relative simplicity of the source structure and the complexity of the light curve during the ESE, our best estimate for this source in the context of the FDJWS scattering model is that the ESE toward 0300+470 may have been caused by the action of a complex (multiple) lens structure along the line of sight.

3.2. *0333+321*

The light curve of 0333+321 exhibits two simple rounded ESE signatures separated in time by approximately 1.7 yr. The source structure of 0333+321 is complex (multiple components of comparable flux density). In the context of the FDJWS model, there are at least two methods for producing the observed light curve: a single lens sequentially passes over two source components, or two lenses pass over a single component.

If a single lens at a distance of 1 kpc is to traverse two source components separated by approximately 1.5 mas in about 1.7 yr, the velocity of the lens must be approximately 4 km s^{-1}. If the lens is 10 kpc distant, then the required velocity is approximately 40 km s^{-1}. In comparison, the shock-induced lenses of Clegg et al. (1988) have much faster velocities (hundreds of kilometers per second). The single-lens explanation requires the lens to move in the same direction as the source component separation. Given a 2.25 GHz component angular size of approximately 1.2 mas (scaled by λ from the 4.99 GHz size) and an approximately 1.5 mas separation between components, the likelihood of the lens passing over two components sequentially is about 40%.

It is possible that the two ESE events are due to the motion of two separate lenses across a single source component. The light curves show simple rounded minima for both events. In the context of the FDJWS model, this implies that the angular size of the lenses is comparable to the angular size of a single source component ($\sim$1.2 mas implying a lens size of $\sim$1.2 AU or $\sim$12 AU for a lens distance of 1 kpc or 10 kpc, respectively), and since the source components are separated by approximately 1.5 mas, the lenses apparently pass over only one of these components (i.e., the lenses move in a direction roughly perpendicular to the direction of the source structure). There is no clear indication as to which of these two cases is the cause of the observed structure in the ESE light curve.

3.3. *1502+106*

The interpretation of the light curve vis-à-vis the VLBI data for this source duplicates almost exactly the discussion for the source 0300+470.

© American Astronomical Society • Provided by the NASA Astrophysics Data System

1996ApJ...468..543F

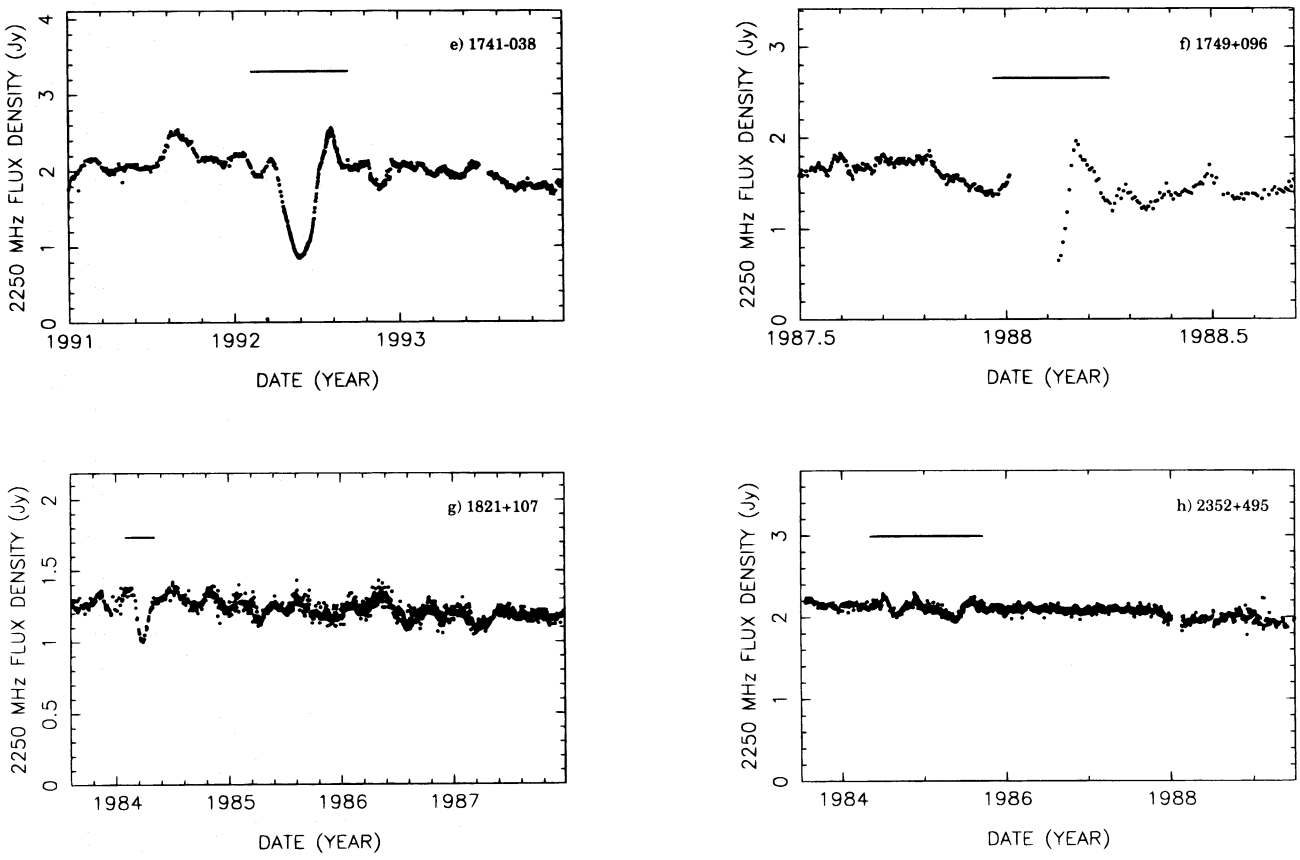

FIG. 9.—*Continued*

3.4. *1611+343*

The light curve for this source exhibits a single, simple flat minimum. The source structure is also simple (a single component at 2.32 GHz). Interpreting the flat minimum in terms of the FDJWS model, the angular size of the lens must be larger than the angular size of the background source. More importantly, the flat minimum implies that the broadening angle, and hence the distribution of electron density fluctuations across the lens, is fairly uniform. The geometric mean angular size at 2.32 GHz is approximately 2.1 mas, implying a lens size of more than 2.1 AU, or more than 21 AU for a lens distance of 1 kpc or 10 kpc, respectively.

3.5. *1741−038*

The light curve for this source exhibits a single, simple rounded minimum. The source structure is also simple (a dominant component containing about 98% of the total flux density at 2.32 GHz). Interpreting the rounded minimum in terms of the FDJWS model, the angular size of the lens must be comparable to the angular size of the background source. The measured angular size of 1741−038 is approximately 0.5 mas at 2.32 GHz, implying a lens size of approximately 0.5 AU or 5 AU for a lens distance of 1 kpc or 10 kpc, respectively.

3.6. *1749+096*

This source is dominated by a single compact core containing about 90% of the total flux density, with an angular size $\lesssim 1$ mas (the core is unresolved along the minor axis) at 2.32 GHz. The beginning and middle of the ESE light curve was not observed at 2.25 GHz because of hardware difficulties. It is apparent from light curves obtained at other frequencies (see FDJWS), however, that 1749+096 probably underwent a single, simple flat minimum event. This implies that the broadening angle, and hence the distribution of electron density fluctuations across the lens, is fairly uniform. Otherwise, all that can be implied from the existing data is that the angular extent of the lens must be considerably larger than the (unknown) angular extent of 1749+096.

3.7. *1821+107*

The light curve for this source exhibits a single, simple rounded minimum. The source structure is also simple (a dominant component containing about 93% of the total flux density at 2.32 GHz). Interpreting the rounded minimum in terms of the FDJWS model, the angular size of the lens must be comparable to the angular size of the background source. The geometric mean angular size of 1821+107 at 2.32 GHz is approximately 0.6 mas, implying a lens size of approximately 0.6 AU or 6 AU for a lens distance of 1 kpc or 10 kpc, respectively.

3.8. *2352+495*

The 4.99 GHz VLBI data show 2352+495 to be a multiple-component source with the two central components dominant. These components have a flux density ratio of roughly 2:1 and contain about 75% of the total flux density. The 2.25 GHz light curve shows a flat minimum

© American Astronomical Society • Provided by the NASA Astrophysics Data System

1996ApJ...468..543F

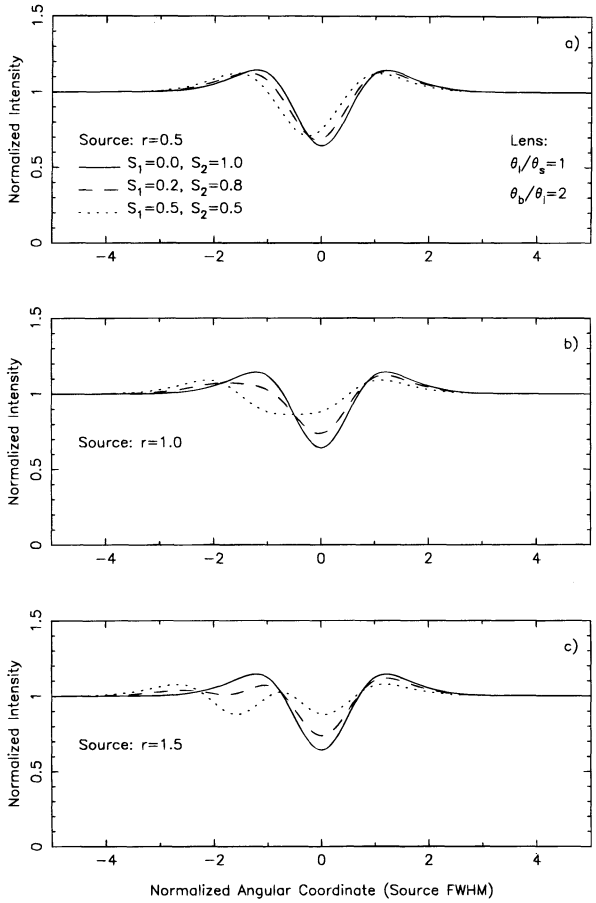

FIG. 10.—Expected radio frequency light curves based on the Fiedler et al. (1994a) scattering model. In this model the scattering lens is assumed to be band-shaped as projected on the sky (cf. Fig. 5 of Fiedler et al. 1994a) and have an angular width θ_l along the small axis of the band. The long axis of the band is assumed to be much greater than θ_l. The relative motion of the lens across the background source is assumed to be along the small axis of the band. Electron density inhomogeneities throughout the lens are assumed to redistribute the radiation from a point source into a Gaussian distribution of angles characterized by an FWHM angular size θ_b. It is also assumed that θ_b is constant across the extent of the scattering lens. This figure represents the case in which the angular size of the scattering lens, θ_l, is approximately equal to the FWHM angular size, θ_s, of the background source. The source brightness distribution is characterized by two Gaussian components, each with FWHM angular size θ_s and flux density S_1 and S_2, respectively. Three cases are considered in each panel: (*solid curve*) $S_1 = 0.0$, $S_2 = 1.0$ (this is the degenerate case and represents a source with only a single component); (*dashed curve*) $S_1 = 0.2$, $S_2 = 0.8$; and (*dotted curve*) $S_1 = 0.5$, $S_2 = 0.5$. The different panels represent the cases in which the two source components are separated by an angular distance: (*a*) $r = 0.5$, (*b*) $r = 1.0$, and (*c*) $r = 1.5$, where the angular units have been normalized by the source size, θ_s. The lens is assumed to move sequentially across the two source components. The form of the lens is the same in each panel.

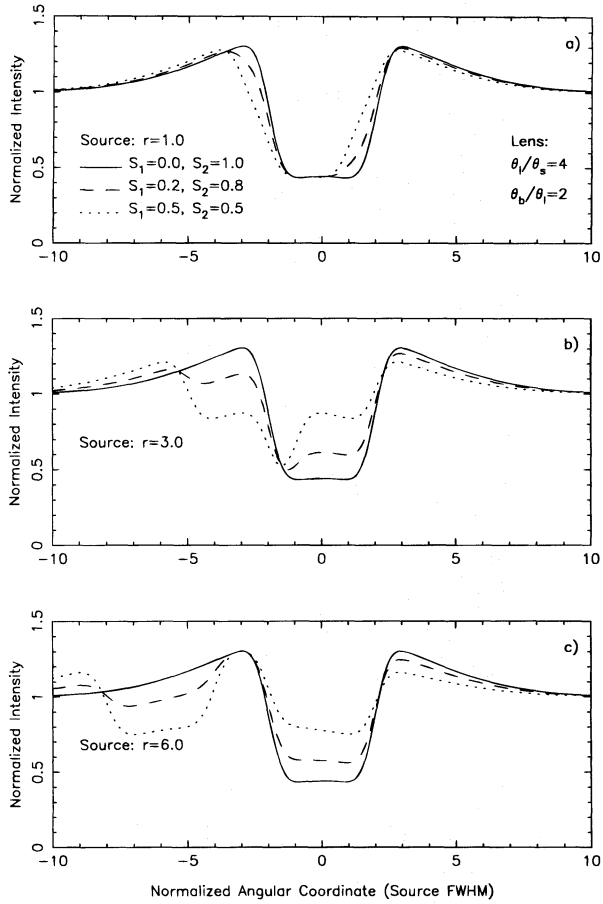

FIG. 11.—The same as Fig. 10, except that the angular size of the scattering lens, θ_l, is approximately 4 times the FWHM angular size, θ_s, of the background source. The different panels represent the cases in which the two source components are separated by an angular distance: (*a*) $r = 1.0$, (*b*) $r = 3.0$, and (*c*) $r = 6.0$, where the angular units have been normalized by the source size, θ_s. The lens is assumed to move sequentially across the two source components. The form of the lens is the same in each panel.

with a central peak, implying that the angular size of the lens is much larger than the angular size of the source components (approximately 1.1 mas and 3.5 mas when scaled from 4.99 GHz to 2.25 GHz as λ). The light curve of 2352+495 can be qualitatively approximated by the case shown in Figure 11*c*, in which a single lens passes over a two-component source, with each component having a similar flux density (*dotted curve*). However, this requires a fortuitous alignment (separation) of the source components such that the edges of their scattering signatures in the light curve add together to produce the central peak. It also requires that the lens move along the direction of the component separation. Furthermore, since the separation between the components is approximately 2 mas at 4.99 GHz, it is implied that the two components have blended together at 2.25 GHz, since their combined angular sizes would be larger than their separation. As with 0300+470 and 1502+106, the more likely situation is that the ESE toward 2352+495 was caused by the action of a complex (multiple) lens structure along the line of sight.

4. SUMMARY

We have presented multiple-epoch, multiple-frequency VLBI observations of eight extragalactic sources whose radio light curves have undergone an ESE. The VLBI observations were made at times during which the sources were not undergoing ESE events. The eight sources show relatively simple intrinsic structure, with one or two dominant components containing the majority of the total flux density, and component angular sizes on the order of several milliarcseconds. Interpretation of the ESE light curves for these sources in the context of the FDJWS statistical scattering model suggests that there is no direct correspondence between intrinsic source structure and the form of the radio light curves during an ESE. Physical sizes of several AU are implied for the scattering lenses for some

© American Astronomical Society • Provided by the NASA Astrophysics Data System

1996ApJ...468..543F

sources. Given the relative simplicity of the intrinsic structure for most of the sources, the results suggest that some of the complexity in the ESE light curves of these sources is due to the complexity of the scattering medium itself. Dedicated flux density monitoring observations as well as VLBI imaging during an ESE are required for further elucidation as to the nature of these elusive events.

We would like to thank the US and European Mark II VLBI networks and the staffs of the participating observatories for making their facilities available for these observations. Basic research in radio interferometry at the Naval Research Laboratory is supported by the Office of Naval Research.

REFERENCES

Altschuler, D. R., Broderick, J. J., Condon, J. J., Dennison, B., Mitchell, K. J., O'Dell, S. L., & Payne, H. E. 1984, AJ, 89, 1784
Antonucci, R. R. J., & Ulvestad, J. S. 1985, ApJ, 294, 158
Browne, I. W. A., Clark, R. R., Moore, P. K., Muxlow, T. W. B., Wilkinson, P. N., Cohen, M. H., & Porcas, R. W. 1982, Nature, 299, 788
Clegg, A. W., Chernoff, D. F., & Cordes, J. M. 1988, in Radio Wave Scattering in the Interstellar Medium, ed. J. M. Cordes, B. J. Rickett, & D. C. Backer (New York: AIP), 174
Clegg, A. W., Fey, A. L., & Fiedler, R. L. 1996, ApJ, 457, L23
Conway, J. E., Pearson, T. J., Readhead, A. C. S., Unwin, S. C., Xu, W., & Mutel, R. L. 1992, ApJ, 396, 62
Dennison, B., Broderick, J. J., O'Dell, S. L., Mitchell, K. J., Altschuler, D. R., Payne, H. E., & Condon, J. J. 1984, ApJ, 281, L55
Fey, A. L., Clegg, A. W., & Fomalont, E. B. 1996, ApJS, 105, 299
Fiedler, R. L., Dennison, B., Johnston, K. J., & Hewish, A. 1987, Nature, 326, 675
Fiedler, R., Dennison, B., Johnston, K. J., Waltman, E. B., & Simon, R. S. 1994a, ApJ, 430, 581 (FDJWS)
Fiedler, R., Pauls, T., Johnston, K. J., & Dennison, B. 1994b, ApJ, 430, 595
Gabuzda, D. C., Cawthorne, T. V., Roberts, D. H., & Wardle, J. F. C. 1992, ApJ, 388, 40
Henstock, D. R., Browne, I. W. A., Wilkinson, P. N., Taylor, G. B., Vermeulen, R. C., Pearson, T. J., & Readhead, A. C. S. 1995, ApJS, 100, 1
Hewitt, A., & Burbidge, G. 1993, ApJS, 87, 451
Hughes, P. A., Aller, H. D., & Aller, M. F. 1992, ApJ, 396, 469
Lawrence, C. R., et al. 1985, ApJ, 296, 458
Marscher, A. P. 1988, ApJ, 334, 552
Marscher, A. P., Broderick, J. J., Padrielli, L., Bartel, N., & Romney, J. D. 1987, ApJ, 319, 456
Napier, P. J., Bagri, D. S., Clark, B. G., Rogers, A. E. E., Romney, J. D., Thompson, A. R., & Walker, R. C. 1994, Proc. IEEE, 82, 658
O'Dea, C. P., Baum, S. A., & Stanghellini, C. 1991, ApJ, 380, 66
Pearson, T. J., & Readhead, A. C. S. 1984, ARA&A, 22, 97
———. 1988, ApJ, 328, 114
Perley, R. A. 1982, AJ, 87, 859
Romani, R. W. 1988, in Radio Wave Scattering in the Interstellar Medium, ed. J. M. Cordes, B. J. Rickett, & D. C. Backer (New York: AIP), 156
Romani, R. W., Blandford, R. D., & Cordes, J. M. 1987, Nature, 328, 324
Romney, J., et al. 1984, A&A, 135, 289
Spangler, S. R., Benson, J. M., Cordes, J. M., Hall, R. B., Jones, T. W., & Johnston, K. J. 1981, AJ, 86, 1155
Stickel, M., Fried, J. W., & Kuehr, H. 1993, A&AS, 98, 393
Taylor, J. H., & Cordes, J. M. 1993, ApJ, 411, 674
Véron-Cetty, M. -P., & Véron, P. 1993, ESO Sci. Rep. No. 13
Wehrle, A. E., Cohen, M. H., Unwin, S. C., Aller, H. D., Aller, M. F., & Nicolson, G. 1992, ApJ, 391, 589
Weiler, K. W., & Johnston, K. J. 1980, MNRAS, 190, 269
Wilkinson, P. N., Polatidis, A. G., Readhead, A. C. S., Xu, W., & Pearson, T. J. 1994, ApJ, 432, L87
Zensus, J. A., Porcas, R. W., & Pauliny-Toth, I. I. K. 1984, A&A, 133, 27

© American Astronomical Society • Provided by the NASA Astrophysics Data System